Journal of Geophysical Research: Space Physics

Pattern and evolution of seismo-ionospheric disturbances following the 2011 Tohoku earthquakes from GPS observations

Shuanggen Jin[1], Rui Jin[1,2], and J. H. Li[1,2]

[1]Shanghai Astronomical Observatory, Chinese Academy of Sciences, Shanghai, China, [2]University of Chinese Academy of Sciences, Beijing, China

Abstract Global Positioning System (GPS) has been widely used to sense crustal deformation and ionospheric anomalies, particularly seismic ionospheric disturbances. In March 2011, the earthquakes with magnitude of up to Mw = 9 occurred in Tohoku near the east coast of Honshu, Japan. The GPS Earth Observation Network (GEONET) in Japan with more than 1200 continuously operating stations provides a unique opportunity to study the detailed seismic ionospheric disturbances. In this paper, the pattern and evolution of seismic ionospheric disturbances following the Tohoku earthquakes are investigated by dense GEONET data, including amplitude, propagation pattern, direction, speed, and evolution. Maximal coseismic ionospheric disturbances are found with up to more than 4 TECU, and the disturbance period is around 10–20 min. The seismic ionospheric effects following the aftershocks are attenuated with the increase of the time and distance between the ionospheric pierce point and the epicenter of the main event, which last more than 2 h. Seismic ionospheric disturbance detected by GPS measurement is not only related to the main shock but also the giant aftershocks. Propagation velocities of the total electron content (TEC) disturbance show a decrease when it spreads 400–600 km away from the epicenter in the north-western direction, where it is just near the west coast of Japan. Furthermore, the TEC disturbance also has obvious directional features. In the first half hour, the TEC disturbance in the southeast direction has the biggest amplitude, while the dominant direction is changed to northwest tens of minutes later. In addition, signals with higher frequencies are existed in seismic TEC variation at the epicenter region but do not appear in the far field.

1. Introduction

Giant earthquakes often result in great loss of economics and lives as well as geohazards, such as tsunami and landslide. Due to the lack of measurement and theoretical understanding for the Earth's interior, it is hard to predict the short-term earthquake's occurrence, location, and magnitude up to now. Getting more insights on earthquake processes will contribute to understand and predict earthquakes. Recently, seismo-ionospheric disturbances can be observed from the Global Positioning System (GPS) [*Calais and Minster*, 1995; *Jin et al.*, 2010; *Afraimovich et al.*, 2010]. The energy released by earthquake affects the Earth's atmosphere in the form of atmospheric wave from seismic vertical deformation and earthquake generated tsunami. The seismic ionospheric disturbance will be amplified dramatically during its upward propagation from the ground to the ionosphere due to the attenuation of atmospheric density [*Artru et al.*, 2001]. With more and more continuous GPS stations, especially in Japan, it provides a great chance to study more details about the seismic atmospheric characteristics and coupling between the solid Earth and atmosphere further.

The seismic ionospheric disturbance was first found from GPS total electron content (TEC) in 1995 [*Calais and Minster*, 1995]. Later numerous studies have been attempted to seek pre- or coseismic anomalies and its physical mechanism [*Liu et al.*, 2004; *Dautermann et al.*, 2007; *Heki and Enomoto*, 2013]. Nowadays the method to extract pre-seismic ionospheric effect is mostly using previous several normal days' TEC to estimate a predicted TEC value based on its statistical behavior for the earthquake days. By comparing the predicted value and the GPS TEC observations, the anomalous TEC variations are regarded as probable pre-seismic TEC disturbances, while its mechanism is still open debated. Different filter methods are applied to the observed GPS TEC time series to obtain the coseismic ionospheric disturbances signals, waves could be induced and spread out after the fault rupture[*Afraimovich et al.*, 2001; *Heki and Ping*, 2005;
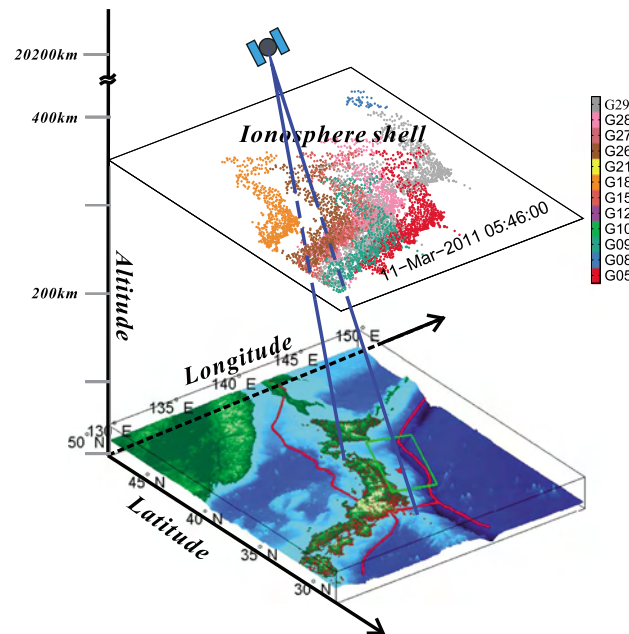
Figure 1. Ground-based ionosphere sounding from dual-frequency GPS in Japan. The colored dots on the assumed ionospheric thin shell show the sub-ionospheric pierce points (SIP) distribution on UTC 05:46, 11 March 2011. The white star is the epicenter location of the 2011 Tohoku earthquake, the red dots on the ground show the distribution of GEONET stations, and the green rectangle is the rupture region estimated by the Tectonics Observatory, California Institute of Technology (http://www.tectonics.caltech.edu).

Heki et al., 2006; Lognonné et al., 2006; Rolland et al., 2011]. However, the Earth's ionosphere has complex and dynamic spatial structure and is affected by the amount of factors, such as geomagnetic field and solar flare. It is difficult to derive accurate pre- and coseismic ionospheric anomalies for regional or global scales. Coseismic ionospheric disturbances sources are normally thought to be near the epicenter, while few GPS stations are located near the epicenter of giant earthquakes, which makes it difficult to get accurate details about the pre-/coseismic ionospheric effects and characteristics.

A giant earthquake with a magnitude of up to 9 occurred in Tohoku near the east coast of Honshu, Japan at 05:46:24 UTC, 11 March 2011, which is the largest earthquake in the last 7 years. It was associated with a number of aftershocks and huge tsunami. The Tohoku earthquake's epicenter is located in 38.297°N, 142.372°E estimated by the US Geological Survey (USGS). It is one of the shallow earthquakes whose focal depth is just 30 km. A dense GPS array of the GEONET with more than 1200 continuously operating stations within 2500 km away from the epicenter provides us a good chance to study the detailed seismic ionospheric effects and propagation characteristics.

A number of seismic ionospheric disturbances for the Tohoku earthquake have been investigated [Tsugawa et al., 2011; Liu et al., 2011]. TEC disturbances spread out to almost all directions from the epicenter with the speed of several hundreds of meters to several kilometers per second. The ionospheric disturbances detected by GPS observations following the Tohoku earthquake showed three modes with different propagation velocities, which may be related to the seismic Rayleigh waves (2–3 km/s), acoustic waves (0.3–1.5 km/s), and tsunami generated gravity waves (0.1–0.3 km/s). Simulated results showed the southeastward ionospheric disturbances, which may be due to the coupling between tsunami and atmosphere [Galvan et al., 2012; Occhipinti et al., 2013]. Two-dimensional simulation of near-field seismic ionospheric effects reproduced the ionospheric hole after the onset of Tohoku earthquake, indicating that the TEC decrease above the epicenter was caused by atmospheric expansion to upper layers derived by the sudden uplift of sea surface during the earthquake [Saito et al., 2011; Kakinami et al., 2012; Shinagawa et al., 2013]. However, these results and simulations were mainly focused on the propagation velocities and the coupling of the tsunami or ground motion and atmosphere. Up to now the pattern and evolution of seismic TEC disturbances following the Tohoku earthquake are not clear in details. In this paper, the pattern and evolution of the disturbance amplitudes, period, propagation speed, and direction features following the Tohoku earthquake are investigated comprehensively using dense GPS observations in Japan. Some discussions on seismic ionospheric characteristics are presented.

2. Ionosphere Monitoring by GPS

As shown in Figure 1, the GEONET with more than 1200 continuously operating GPS stations was established in 1996 by the Geospatial Information Authority of Japan with the aim of monitoring crustal deformation.

GPS ionosphere monitoring is one of the significant applications. The average distance between GEONET stations is about 25–30 km. Therefore, the dense GEONET provides us a good opportunity to monitor the Earth's ionosphere with high precision and resolution.

The total electron content (TEC) can be derived from the dual frequency GPS observations as the following equation [*Jin et al.*, 2008]:

$$
\begin{aligned}
STEC &= \frac{f_1^2 f_2^2}{40.28\left(f_1^2 - f_2^2\right)} \left(L_1 - L_2 + \lambda_1(N_1 + b_1) - \lambda_2(N_2 + b_2) + \varepsilon\right) \\
&= \frac{f_1^2 f_2^2}{40.28\left(f_2^2 - f_1^2\right)} \left(P_1 - P_2 - (d_1 - d_2) + \varepsilon\right)
\end{aligned}
\tag{1}
$$

where $STEC$ is the slant TEC, f is the carrier phase frequency, L and P are the carrier phase and pseudorange observations, respectively, λ is the signal wavelength, N is the ambiguity, b and d are the instrument biases for carrier phase and pseudorange, and ε is the other residuals. The vertical TEC can be converted from STEC by [*Klobuchar*, 1987]:

$$
vTEC = STEC * \cos\left(\arcsin\left(\frac{R \sin z}{R + H}\right)\right)
\tag{2}
$$

where R is the Earth radius, H is the thin shell height of the ionosphere, and z is the satellite's elevation angle. Here we choose the height with the maximum electron density as the shell height. We determine the height (268 km) with ionsonde data in Japan on 11 March provided by Space Physics Interactive Data Resource (SPIDR).

In Figure 1, the colorful dots on the assumed ionospheric thin shell show the sub-ionospheric pierce points (SIP) distribution from GEONET at UTC 05:46, 11 March 2011, where the different colorful dots are corresponding to the SIP distribution for different GPS satellites. The white star is the location of the Tohoku earthquake's epicenter, the red dots on the ground terrain stand for the GEONET station, and the green rectangle is the rupture region estimated by the Tectonics Observatory, California Institute of Technology (http://www.tectonics.caltech.edu). Since the dense SIP focus around the epicenter, the detailed seismic ionospheric disturbances can be obtained following the Tohoku earthquake. Here, continuous observations of more than 1200 stations are collected with the sampling interval of 30 s. Using the method mentioned above, the precise vertical TEC series at SIP around the epicenter are obtained with a 30 s interval. The precision of GPS carrier phase measurement is less than 1 mm. According to the error propagation law, the measurement error of TEC is about 0.01 TECU. The detrended TEC in quiet condition is nearly the random noise, which is dominated by the measurement error. In quiet condition the detrended TEC value will usually fall into the three-sigma range of about −0.03–0.03 TECU. When the detrended TEC values are out of this range, the TEC anomalies could be detected. The high precision and high temporal-spatial resolution ionospheric TEC from GEONET provides the opportunity to discuss the detailed seismic ionospheric pattern and evolution. The detailed TEC disturbances following the earthquake are investigated and discussed in the next section.

3. Results and Discussion

In this section, the ionospheric disturbances following the Tohoku earthquake with GEONET data are analyzed in details, including the pattern and evolution of the disturbance amplitudes, spectrograms, propagation speed, and direction. The times in GEONET data are corrected by adding the difference between UTC and GPS time with −15 s on 11 March 2011 according to the International Earth Rotation and References Systems Service (IERS) Bulletins (http://hpiers.obspm.fr/eop-pc/). In order to degrade the multipath effects and the error of mapping function, measurements with low satellite elevation angles (less than 10° if not specified in following) are not used. In order to remove the TEC trend and high frequency fluctuations and other noises, the detrended TEC series are filtered with four-order zero-phase shift Butterworth filter that is designed with a most flat frequency response in the passband without phase shift.
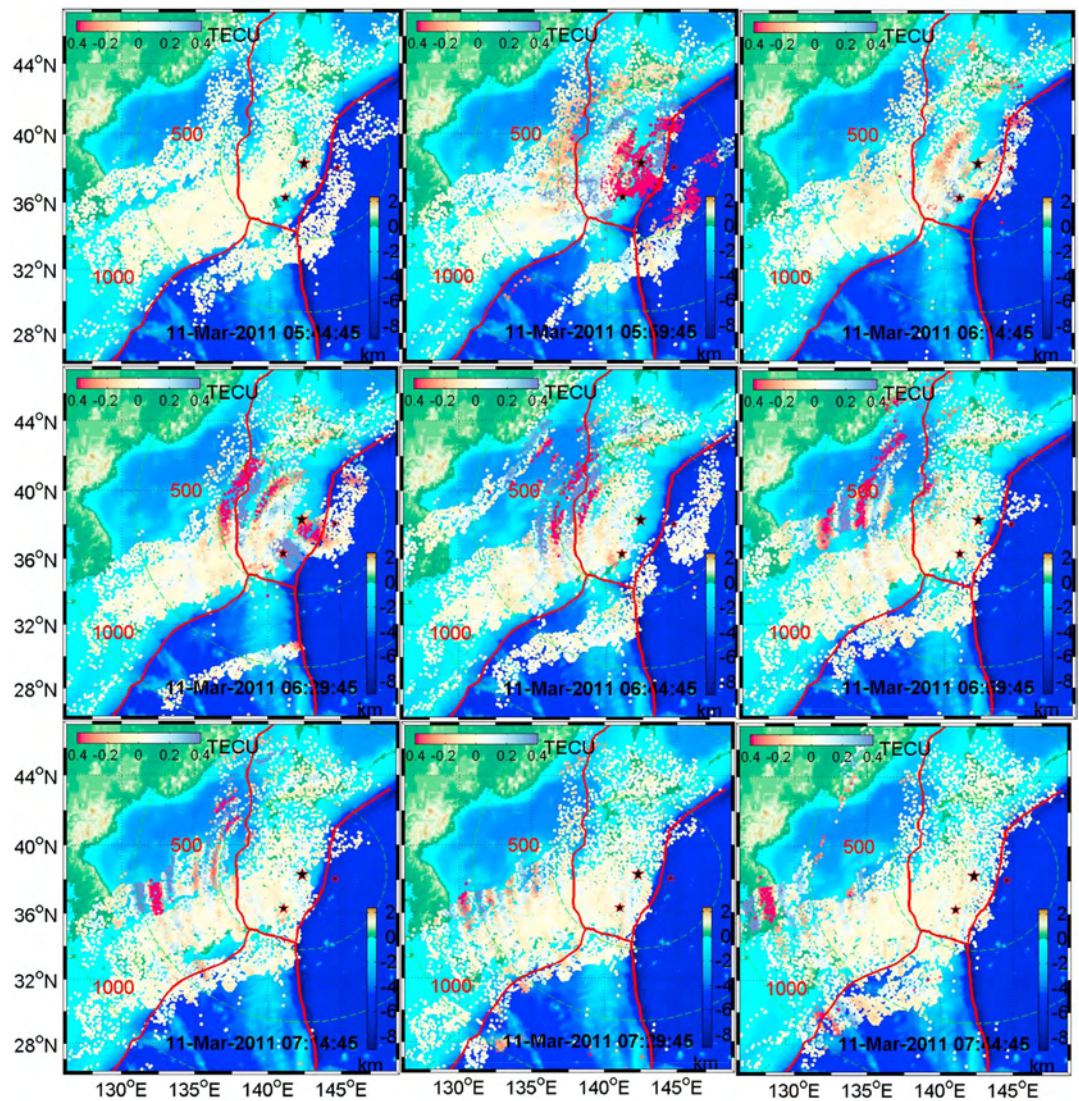
Figure 2. Detrended total electron content (TEC) variations following the main shock in Japan with a 15 min interval. The amplitude is shown in color. The three stars (the symbol size is proportional to magnitude) stand for the location of the main shock epicenter and the two aftershocks with Mw > 7 during the 2011 Tohoku earthquake. The topographic data are provided by the US National Geophysical Data Center (NGDC). Here the 0 km is corresponding to the mean sea level. The red line is the plate boundary [*Jin et al.*, 2007].

3.1. TEC Anomalies Following the Tohoku Earthquake

Figure 2 shows the detrended TEC maps derived from GEONET data with a 15 min interval following the Tohoku earthquake. The topography is plotted in this region from the US National Geophysical Data Center as the background, in order to show the topography influence on TEC disturbances. Here the TEC series obtained by GEONET dual frequencies GPS measurements are filtered with a 1–15 mHz window for detrending. The trend is mainly caused by SIP's motion and ionospheric background changes. Here we chose the 15 mHz as the high cut-off frequency in consideration of the 30 s interval of the GEONET ionospheric monitoring, avoiding the aliasing in signal processing. Dramatic negative and positive disturbances appeared near the epicenter around UTC 6:00, which were mainly on the two sides of the rupture as shown in Figure 2. The Tohoku earthquake was resulted from a thrust between the Pacific and North America plates. The disturbance in the epicenter region seems to be related to sea level change caused by the thrust directly, and the source of seismic ionospheric disturbances is located in the rupture region. The seismic ionospheric disturbance following the 2011 Tohoku earthquake derived by the Butterworth filter agrees well with the result based on moving average detrend [*Tsugawa et al.*, 2011].
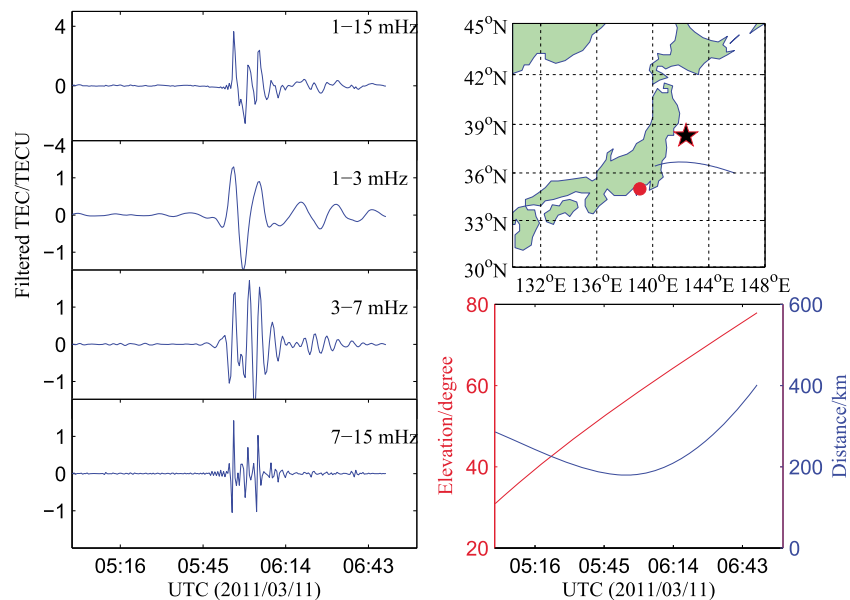
Figure 3. TEC disturbances observed by the station 2106 with PRN 26 on 11 March 2013. The left panel is the filtered vertical TEC, and the right panel describes the observation geometry. The blue line in the right top panel is the SIP trajectory. The star and circle show the location of the epicenter and the station 2016. The right bottom panel shows the satellites' elevation angle (red line) and the geodetic distance between the SIP and epicenter (blue line).

The ionospheric disturbance spreads out from the epicenter as a quasi-circular propagation pattern with the time. The large amplitudes are up to 3–4 TECU as shown in Figure 3. The strong disturbances last nearly 2 h from UTC 6:00 to 8:00, while in most areas the disturbance amplitudes are 0.1–0.4 TECU, which are much larger than the normal level. The disturbances with large amplitudes occurred above the Sea of Japan, except the epicenter region. Above the Sea of Japan, the relatively strong disturbances are found at UTC 07:16 and UTC 07:46. Till UTC 08:16, the TEC recovers to the state before the main shock as shown by the first and last subfigures in Figure 2. The TEC disturbance has a second enhancement around UTC 06:15–06:30 as shown by the series of TEC disturbance maps. More details about this point will be discussed in the next section.

3.2. Variation of TEC Disturbance Amplitudes

Figure 3 is an example of TEC disturbance amplitudes following the Tohoku earthquake detected by the line-of-sight (LOS) between the station 2106 and GPS satellite 26. The left panel is the filtered TEC with different band-pass windows, and the right panel shows the observation geometry. Obvious disturbance appears several minutes after the main shock in all the four filtered TEC series. For the 1–15 mHz, it is the detectable frequency range of 30 s interval GPS measurement for ionospheric disturbance. Here we chose 1 mHz as a threshold to remove the background TEC variation. As shown in the right panel of Figure 3, the arc has a good view on the ionosphere following the Tohoku earthquake in the near field within 400 km away from the epicenter. The disturbance shows the dramatic characteristic like impulsion wave. The disturbance amplitude decreases rapidly with the increase of the time and the distance of SIP's location and the epicentre. The maximum amplitude is up to about 4 TECU for 1–15 mHz. *Rolland et al.* [2011] pointed out that the LOS slant TEC with low elevation angle is more sensible to the seismic ionospheric disturbances. However, here for the vicinity of the epicenter, the TEC series seem not to have a positive correlation with the satellite elevation angle as shown in the right bottom panel of Figure 3. The distance and time variation should be the main factors for the disturbance amplitude, and the disturbance even lasts until to UTC 8:00. The disturbance amplitudes are even larger than 1 TECU not only in 3–7 mHz but also the two other bands in the first half hour after the main shock. The ionospheric disturbance in 1–3 mHz has larger amplitude than the others about the second half hour, although the 3–7 mHz filtered TEC series appear a second enhancement. The multi-frequency disturbances are induced after the earthquake in the vicinity of the epicenter, and GPS ionospheric
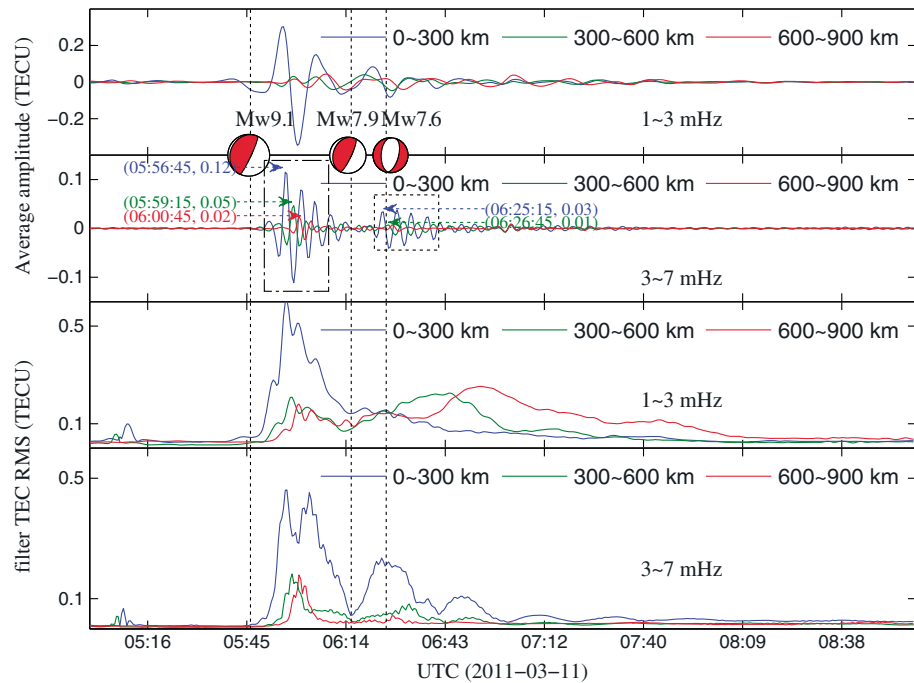
Figure 4. The mean value and root mean square of filtered TEC with the different band-pass windows from near to far field during UTC 5:00–9:00 in March 2011. The three dot lines are corresponding to the time of the main shock and the two aftershocks with Mw > 7. The focal mechanism solution is provided by the Global Centroid-Moment-Tensor (CMT) Project [*Ekström et al.*, 2012].

measurement near the epicenter can detect the acoustic wave and wave related to the Rayleigh wave (3–7 mHz) and tsunami-generated gravity wave (<3 mHz) [*Matsumura et al.*, 2011; *Occhipinti et al.*, 2013] but also higher frequencies signal (7–15 mHz).

Figure 4 shows the temporal variations of the mean value and the RMS (root mean square) of the filtered TEC series from the vicinity of the main shock epicenter to the far field. The focal mechanism solutions of the main shock and the two aftershocks with Mw > 7, whose onsets are UTC 05:46, UTC 06:15, and UTC 06:25, are marked by the beach balls in the upper subfigure. There epicenter locations are marked in Figure 2. Here we do not discuss the signal between 7 and 15 mHz, because the magnitude of its mean amplitude variation in one region is too small in consideration of the GPS measurement noise. In general, the ionospheric variation in this area is recovered to the normal level at around UTC 08:00. Seismic ionospheric disturbance with 1–3 mHz has a larger mean amplitude comparing to the one with 3–7 mHz. The average disturbance amplitude decreases dramatically during the ionospheric disturbance away from the epicenter. Comparing to the disturbance in 1–3 mHz, the mean amplitude of disturbance in 3–7 mHz nearly recovers to zero for the region out of 300 km away from the main shock epicenter. It seems that the high-frequency disturbance attenuates faster as its spreading out. It has been found that there is a second ionospheric disturbance with 3–7 mHz within 300 km away from the epicenter (almost covering the rupture region), which appears several minutes after the first giant aftershock (Mw 7.9) and reaches the max in 10 min that is similar to the situation of the main shock ionospheric anomaly variation, as shown in the mean amplitude and RMS of the filtered TEC series.

As we known, ionospheric disturbances related to several types of waves, such as Rayleigh wave, acoustic wave, tsunami-generated gravity wave, etc., are probably induced following the giant earthquake [*Ducic et al.*, 2003; *Artru et al.*, 2004; *Occhipinti et al.*, 2013]. The Rayleigh and acoustic waves propagate with the speed of about 2–3 km/s and around 1 km/s [*Heki et al.*, 2006]. The propagation distance is far more than 300 km till to UTC 6:30. Figure 5 is the sea level change in the vicinity of the epicenter recorded by Bottom Pressure Records (BPR). Two obvious disturbances exist in all three bottom ocean pressure residual series. The first one with a speed of 3071 m/s should be related to the seismic Rayleigh wave, while the second
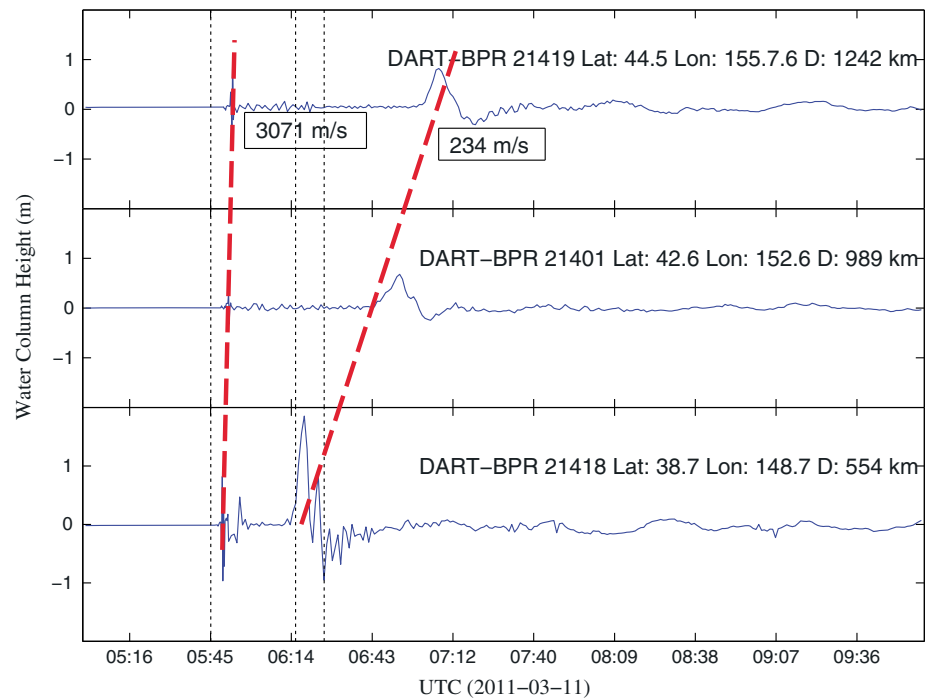
Figure 5. The sea level variation recorded by three near field Bottom Pressure Recorders (BPR).The data are provided by Deep-ocean Assessment and Reporting of Tsunami(DART) buoys (http://www.ndbc.noaa.gov/). The slopes of the two red dash lines show the horizontal velocities (3071 and 234 m/s, based on linear fitting) of two disturbances. The three dot lines are the same with Figure 4.

disturbance with a speed of 234 m/s should be related to the tsunami propagation, which is the source of the tsunami-generated gravity wave in the open sea. The tsunami has been propagating to more than 500 km away from the epicenter. Although the tsunami-generated gravity wave along the tsunami propagates slowly, the tsunami signal can be visible in the ionosphere at least 500 km away from the epicenter according to Occhipinti et al.'s simulation [*Occhipinti et al.*, 2013]. Furthermore, from the perspective of TEC disturbance frequency, the tsunami-generated gravity wave is less than 3 mHz, while the Brünt-Vaïsalla frequency is in order of 3 mHz. The disturbances shown in the dotted rectangle, as shown in the second axis, should not be related to the three probable waves induced by the main shock directly. Considering the time shifts corresponding to peaks of 3–7 mHz regional average TEC disturbances series, the waves spread out from the near field to the far field with speeds of several kilometers per second, which are more agreement with the Rayleigh wave. The disturbances not only in the dash-dotted rectangle but also in the dotted rectangle propagate much faster than the tsunami-gravity wave. When we assume the aftershock epicenter as the source for the second ionospheric disturbance, the situation is similar with propagating much faster than the tsunami gravity wave. It is difficult to distinguish the ionospheric effect induced by the two giant earthquakes because their onset interval is just 10 min. Note that the decrease trends of the average amplitudes corresponding to the first and second disturbances presented in the blue line in the second subfigure of Figure 4 show some subtle difference. The amplitude variation of the second one does not attenuate immediately but remains at the high level till almost 10 min (shown as the first to the third positive peak in the second ionospheric disturbance mentioned above) after the second giant aftershock (Mw 7.6). Similar phenomenon is found in the filtered TEC RMS series for 0–300 km in 3–7 mHz. The second giant aftershock (Mw 7.6) should be also one probable source of the ionospheric disturbance marked by the dotted rectangle in Figure 4. Therefore the second ionospheric disturbance marked by a dotted rectangle in Figure 4 is related to the giant aftershocks, especially for the earthquake with Mw 7.9, which has the similar focal mechnism solution, while there is no such feature for 1–3 mHz. Besides the two biggest earthquakes, there is an amount of aftershocks following the main shock with Mw < 7, but the TEC disturbance amplitudes have no significant variation. The RMS of the filtered TEC amplitude becomes bigger
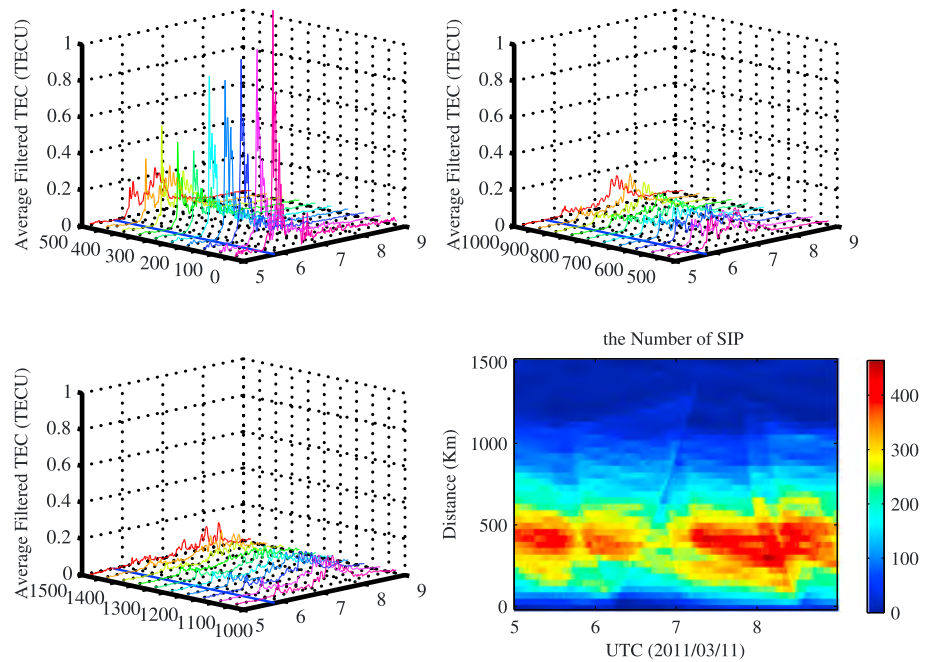
Figure 6. Average amplitudes of the absolute filtered TEC variations with the distance to the epicenter during UTC05:00–09:00, 0–500 km (top left), 500–1000 (top right), and 1000–1500 km (bottom left). The blue line is the onset of the Tohoku earthquake in the Distance-UTC plane. In the right bottom, the color scale is the number of SIP at corresponding time and regions.

in far field after UTC 6:30 as shown in Figure 4. The feature maybe related to two factors. One is that the ionosphere above the epicenter recovers to the quiet condition gradually with the time. The other one is that the directional diversity becomes dramatic for far field.

Another slight but visible anomalies show in the amplitude average and RMS series of 0–300 km in 1–3 mHz around UTC 05:10, which is similar to *Heki and Enomoto* [2013] with an enhanced TEC in dozens of minutes before the giant earthquake main shock. However, this anomaly does not last to the onset of the earthquake main shock but just exists with several minutes. Their results were based on the polynomial fitting residual of TEC series, and our results are based on the filtering TEC series. The polynomial fitting residual will be affected by the whole arc's measurement. The post-seismic disturbances have a great impact on the polynomial fitting result, while our statistical results have no such effects. The pre-seismic TEC disturbances of the Tohoku earthquake are also found significantly but are weak when compared to the post-seismic disturbances. However, the geomagnetic is not quiet on 11 March registered in Dst, Ap, and AE index series as shown in Figure 11. The relationship among the ionospheric disturbance, geomagnetic variation, and the giant earthquake still needs to be studied in the near future.

Figure 6 shows the relationship between the time and distances between the SIP's location and epicenter (here the satellite elevation angle threshold is set as 30°). The blue line is the onset of the Tohoku earthquake in the Distance-UTC plane. The right bottom is the number of SIP of corresponding time and regions. The right bottom panel in Figure 6 shows SIP numbers at special epoch. Here we use the absolute value of the filtered TEC to get a view of the attenuation of seismic ionospheric disturbance. For most areas during this period, ionosphere monitoring from GEONET is available, except a few epochs near the epicenter and 1500 km far from the epicenter. The strongest disturbances mainly appeared in the near field. The seismic ionospheric disturbance amplitudes decreased dramatically with the SIP's location far away from the epicenter, especially in the near field. Obvious disturbances are found till UTC 09:00 and 1500 km far away from the epicenter, while the average filtered TEC for the region with 50 km interval is even more than 1 TECU and decreases to about 0.2 TECU as it spreads out of 500 km away from the epicenter. It is interesting to see that the amplitude attenuation becomes slower when the ionospheric disturbance spreads out of 500 km. From 500 to 1000 km, the average amplitudes show no dramatic decrease but just have the time delay.
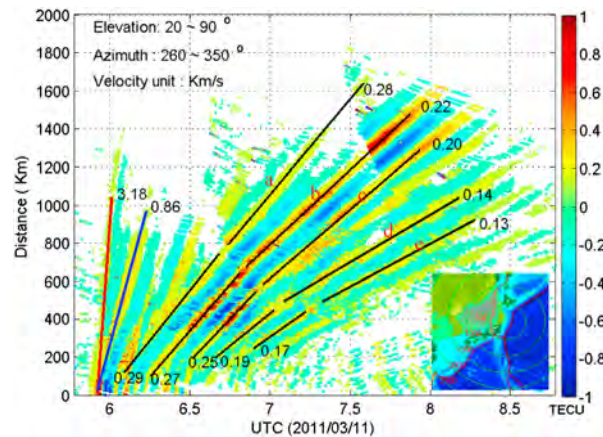
Figure 7. Travel time diagram of post-seismic TEC disturbances following the Tohoku earthquake on 11 March 2011. The SIP with azimuth angles of 260–350° and satellite elevation angles of 20–90° are used. The disturbance amplitude is described by the scaled color. The bottom right figure shows the SIP location area with a yellow sector patch. The red circles are equidistance line to the epicenter corresponding to 500–2500 km with a 500 km interval.

In general the seismic ionospheric disturbances following the Tohoku earthquake are attenuated with the increase of the time and the distances between SIP and epicenter. The amplitudes can reach up to 1–4 TECU. Near the epicenter, the disturbances are trigged by not only the main shock but also the two strongest aftershocks. The average disturbance amplitudes decrease rapidly from the epicenter to 500 km away, while the decrease becomes much more slowly at the 500–1500 km region.

3.3. Propagation Characteristics of TEC Disturbances

The propagation characteristics of post-seismic ionospheric disturbances are further investigated following the Tohoku earthquake. Since the TEC disturbances in the southeast part and the epicentre area have been discussed [*Galvan et al.*, 2012; *Occhipinti et al.*, 2013; *Shinagawa et al.*, 2013], we will focus on the northwest part with dense observations and the strongest disturbances except near the epicenter. The SIP with azimuth angles of 260–350° and satellite elevation angles of 20–90° are used. Figure 7 shows the propagation patterns corresponding to Rayleigh wave at 3.18 km/s, acoustic wave at 0.86 km/s, and gravity wave at 0.1–0.3 km/s. The disturbance amplitude is described by the scaled color. The disturbances of gravity wave have the longest duration. When the disturbances spread out by 200–400 km away, the disturbances are enhanced obviously. Moreover, the propagation velocities have a slight decrease in the area of 500–600 km as shown by waves a–e. The corresponding disturbance region just appears nearby the west coast of Japan as shown in the bottom right figure. The disturbances in this area are caused by the persisting of tsunami generated gravity waves beyond the east coast of Japan [*Galvan et al.*, 2012]. According to the *Occhipinti et al.* [2013] simulation, the horizontal velocity of tsunami-generated wave has a deceleration. Here the occurrence time of slowing horizontal velocity (50–100 min) and the region (400–600 km away from the epicentre) just are corresponding to the time and region of the tsunami-generated wave propagating to the altitude of around 125 km (the isothermal hypothesis ceases need to be valid), where the horizontal velocity of tsunami-generated wave has a strong deceleration. The slowing propagation of the TEC disturbance detected by the GPS ionospheric measurements in the northwest direction should be related to the effect of gravity wave upward propagation. An amplitude enhancement of the ionospheric disturbance appears around 200–400 km away from the epicenter. The amplitude variations along one stripe, which should be induced by the same disturbance source, do not simply attenuate as its spreading out, especially for the stripe b, whose amplitudes show no obvious attenuation even at 1400 km distance. As we know, the electron density increases dramatically from the ground to 300 km altitude. Although the variation of atmospheric mass density will attenuate, the electron density variation could be still dramatic because the electron density increases as the wave up propagation. Note that the tsunami-generated wave in deeper ocean has a higher propagation speed [*Occhipinti et al.*, 2013]. From waves a–e, which are corresponding to different tsunami waves, the horizontal velocities decrease gradually should be related to the tsunami's propagation form the source to the coast.

3.4. TEC Disturbance Spectrogram

Figure 8 presents TEC disturbance time series and spectrograms around the epicenter from UTC 05:00 to UTC 09:00. Here the one-sided normalized power spectral density (PSD) is computed using the short-time Fourier transform. The length of the window is set as 30 min. In the left upper panel, the star is the location of epicenter, and the circle is the location of the corresponding GEONET station. The black line is SIP's
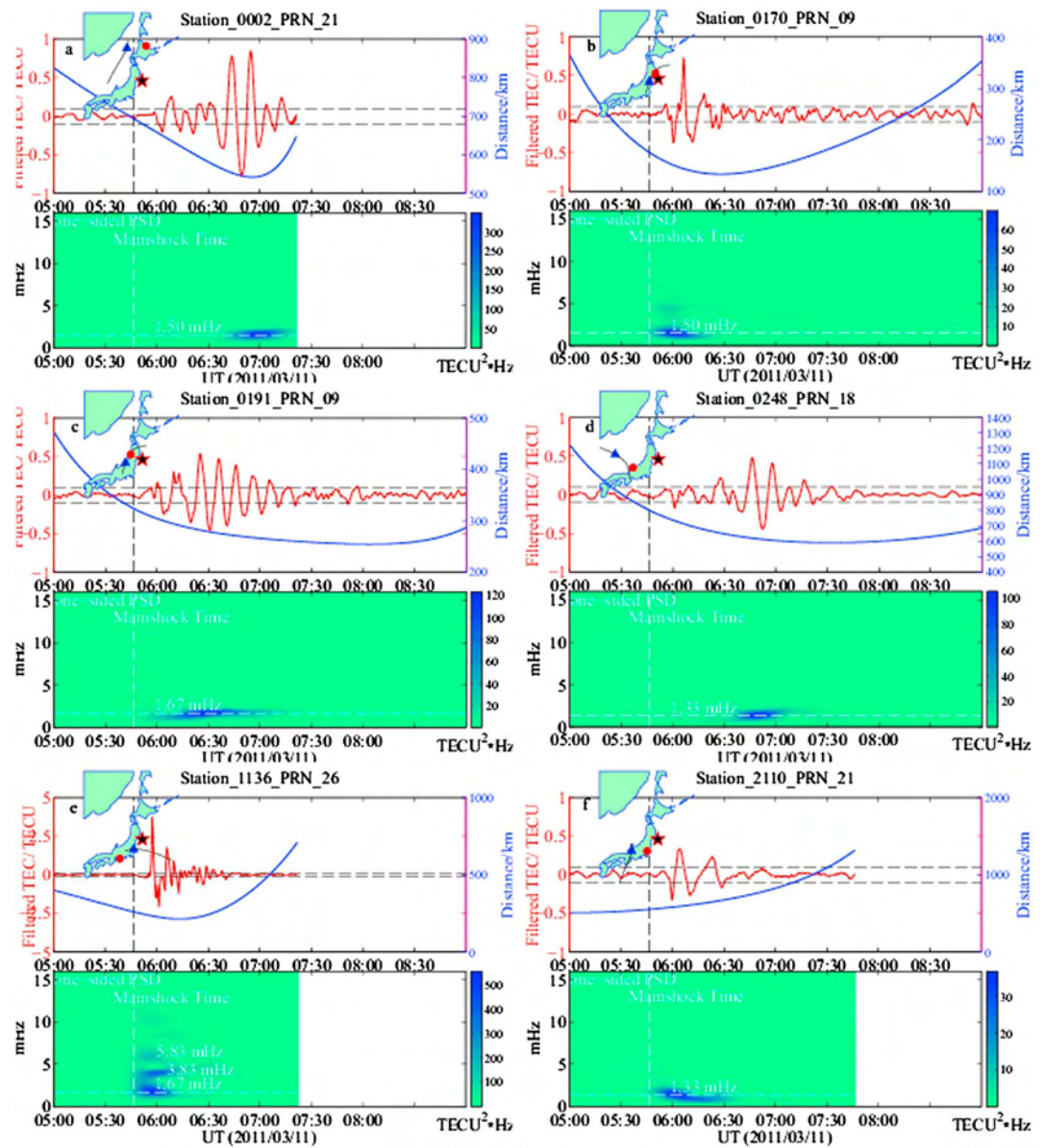
Figure 8. TEC disturbances and spectrograms around the epicenter in several hours after the Tohoku earthquake. Here the one-sided normalized power spectral density (PSD) is computed using the short-time Fourier transform. The length of the window is set as 30 min. In the left upper panel, the star is the location of the epicenter, and the circle is the location of the corresponding GEONET station. The black line is the SIP's tracks, and the triangle is the SIP location at the onset of the Tohoku earthquake. The paralleled horizontal dash lines are the reference lines between 0.1 and −0.1 TECU.

tracks, and the triangle is the SIP location at the onset of the Tohoku earthquake. The paralleled horizontal dash lines are the reference lines between 0.1 and −0.1 TECU. Since the interval of GEONET observation is 30 s, we could detect the signal with a frequency of less than 16.7 mHz according to the Nyquist theorem. In general, the frequency with the largest power spectral density is around 1.3–1.8 mHz (about 10 min period) for all the TEC time series corresponding to different directions of the epicenter, and the signal duration is about dozens of minutes, although their propagation velocities are different. Another two signals with 3.83 and 5.83 mHz appeared in the time series, which are the TEC disturbances near the epicenter. While in the far field, there are no signals with these two frequencies. Therefore, the high-frequency disturbances are attenuated with its propagation.
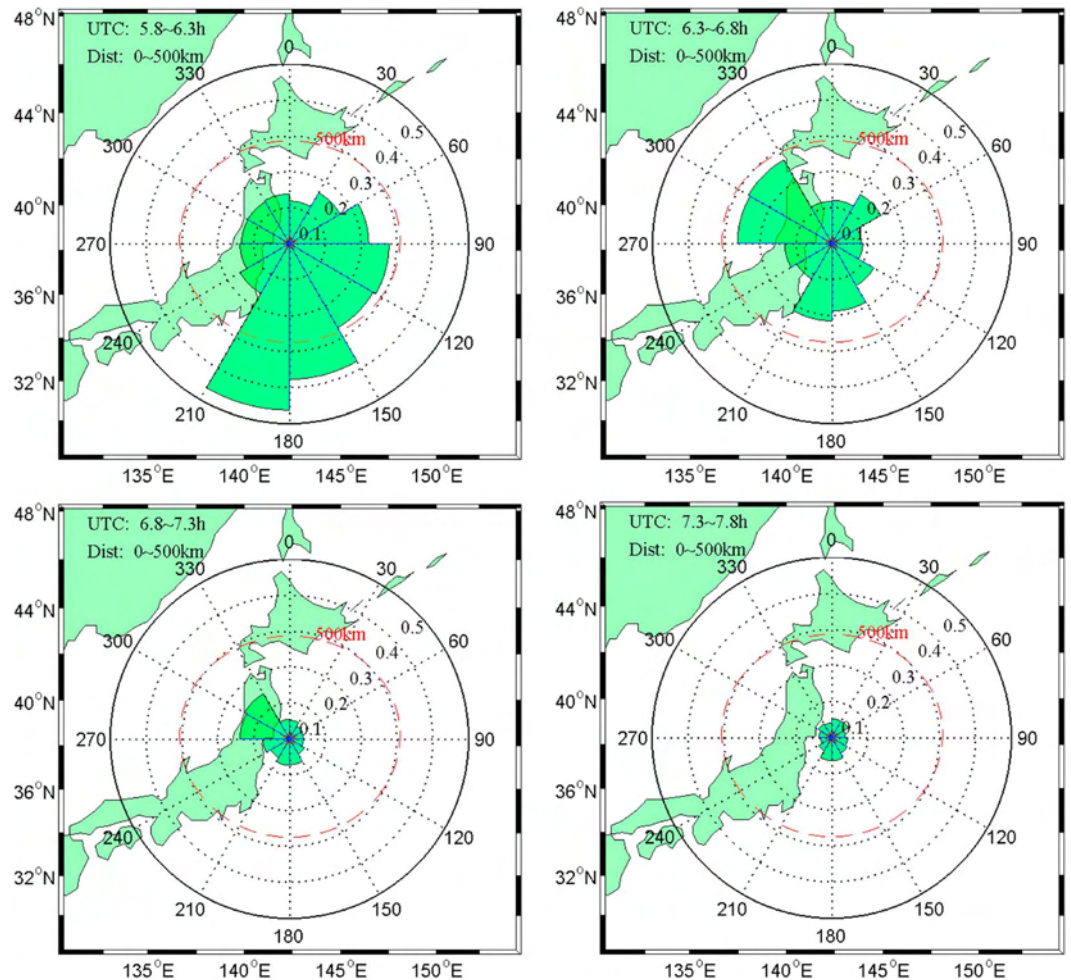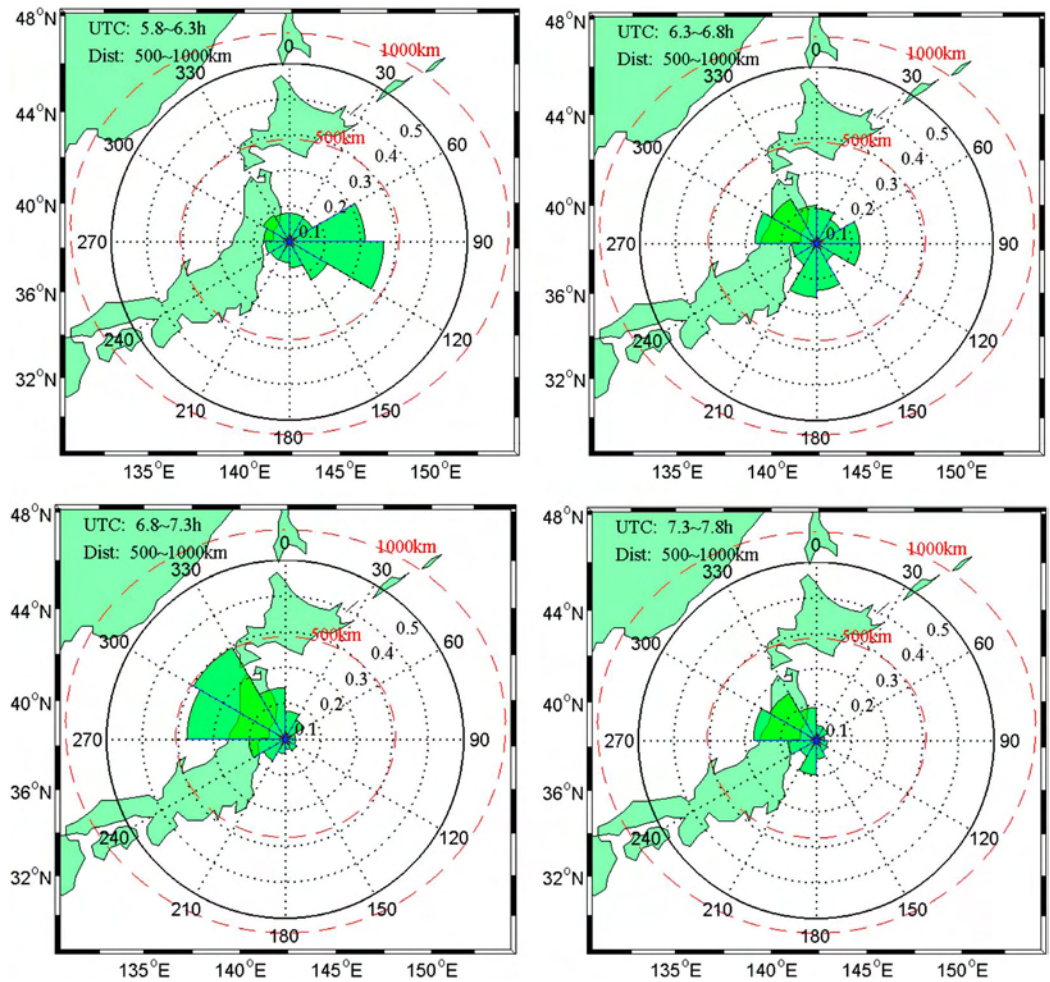
Figure 9. Average amplitude of the absolute detrended TEC in different directions in 0–500 km from the epicenter. Here the radius of the sector patch stands for the average amplitude.

3.5. Directional Feature Changes of TEC Disturbance Amplitudes

Figures 9 and 10 show the average amplitudes of the ionospheric disturbances following the Tohoku earthquake in different directions with respect to the epicenter at a 30 min interval from UTC 05:46 to UTC07:46. The radius of the circles stands for the average amplitude. In the near field (0–500 km), stronger disturbances appear above the open ocean in the first half hour, while in the next hour, the largest amplitude is in the northwest direction. The average amplitudes decrease to about 0.05 TECU at UTC 7.3–7.8. The disturbances in southeast are related to the earthquake generated tsunami [*Galvan et al.*, 2012]. The amplitudes in southeast decrease sharply at half an hour later, which may be related to the tsunami spreading out of 500 km in the open ocean, while no tsunami drives after about half an hour in the near field as shown in Figure 5. In the northwest direction, the amplitudes reach up to the maximum value in the second half hour. Tsunami horizontal velocities decrease with the increase of the oceanic depth [*Occhipinti et al.*, 2013]. Unlike the south-eastward tsunami, the north-westward tsunami velocity, which meets just half of the opposite direction, goes down with its propagation. Furthermore, the tsunami amplitude increases with the decrease of the oceanic depth. The average amplitude variations should be dominated by the sea level displacement by the earthquake generated tsunami.

For the far-field area with 500–1000 km, the variation trend of most disturbed directions is similar with the near field, while amplitudes reach up to maximum value in UTC 6.8–7.3 in the northwest direction, and the average amplitude is still much higher than the quiet condition during UTC 7.3–7.8. In general, the

Figure 10. Average amplitude of the absolute detrended TEC in different directions in 500–1000 km from the epicenter. The radius of the sector patch shows the average amplitude.

amplitudes are smaller than the near field with the propagation attenuation, except in the northwest direction. The large amplitude in the northwest direction for 500–1000 km should be persisted obliquely due to upward propagation of tsunami-generated gravity wave as discussed in the previous section.

3.6. Geomagnetic Activity and Solar Radio Flux in March 2011

As we know, the geomagnetic and solar activities affect the Earth's ionosphere ionization and dynamics. Figure 11 shows the geomagnetic index and solar radio flux variations in March 2011. The Dst index is derived from the H components of the geomagnetic field observed by four magnetic observatories located at tropics nearby which are sufficiently far from the auroral and equatorial electrojets. The AE index is geomagnetic H components derived from 12 stations located in the auroral zone, which is the indictor of electric currents flowing in the high-latitude ionosphere. The Ap is the linear scale of the Kp index and monitors geomagnetic disturbance at the subauroral region. The solar radio flux of 10.7 cm reflects the solar activities in corresponding days. The Dst, AE, and Ap index have some disturbances during the Tohoku earthquake. *Heki and Enomoto* [2013] checked the TEC series and found no disturbances at hourly or minutely level on 11 March 2011. All Dst, AE, and Ap showed similar disturbances around the earthquake days, indicating that the geomagnetic disturbances is not regional effects. However, almost all TEC anomalies are found at hourly or minutely level, which are related to the 2011 Tohoku earthquake. As for the relationship between the geomagnetic disturbances and the Tohoku earthquake, it will be further discussed in the future. The solar activity is quiet on the earthquake day, and the TEC response to the solar activities is instantaneous [*Mansoori et al.*, 2013].
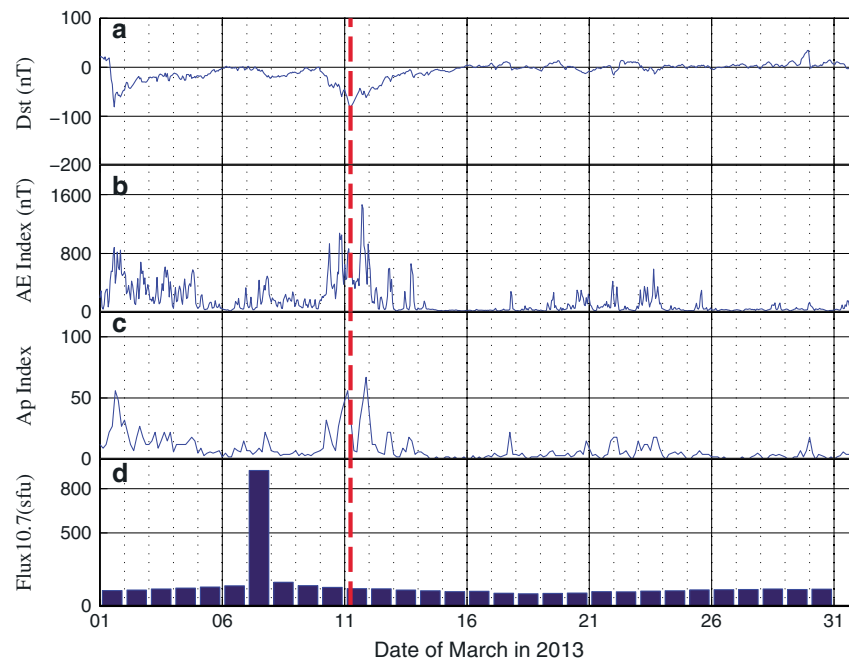
Figure 11. Geomagnetic index and solar radio flux at the wavelength of 10.7 cm variation in March 2013. The Dst (a) and AE (b) index series in March 2011 are provided by the World Data Centre (WDC) for Geomagnetism, Kyoto (http://wdc.kugi.kyoto-u.ac.jp). The Ap (c) index is from GeoForchungsZentrum (GFZ) (http://www.gfz-potsdam.de/), and solar radio flux (d) at the wavelength of 10.7 cm is provided by the Space Physics Interactive Data Resource (SPIDR) (http://spidr.ngdc.noaa.gov).

4. Summary and Conclusion

In this study, we investigate the seismic ionospheric disturbance characteristics following the Tohoku earthquakes in details using the GPS data from GEONET, including disturbance amplitude, propagation speed and direction, spectrogram, and evolution. Except near the epicenter, the most disturbed region is located in the northwest, mainly above the Sea of Japan. The disturbed TEC almost recovers to the pre-earthquake state in 2 h after the main shock. The post-seismic ionospheric effects are related to not only the main shock but also the two strongest aftershocks. This point may be meaningful for us to seek a more realistic source function of the seismic ionospheric effect that not only considers the effect of the main shock but also the aftershocks. A slight disturbance appeared before the onset of Tohoku earthquake in the near field, which may be a precursor of the giant earthquake, but still needs a further validation. Disturbance amplitude decreases rapidly in 0–500 km far from the epicenter. The ionospheric effects following the Tohoku earthquake are attenuated with the increase of the time and distance between the SIP and the epicenter, especially in the near field. The disturbance spreads out with three patterns, which are related to the Rayleigh wave, acoustic wave, and tsunami-generated wave. In the northwest area, the disturbances are enhanced obviously when the disturbances propagated to 200–400 km, and the propagation velocities decrease in the area of 500–600 km, which are related to the decrease of its horizontal velocities as upward propagation from the ground to the ionosphere. The frequency of detrended TEC perturbation with the largest PSD is 1.3–1.8 mHz. Signals with higher frequencies (3.83 and 5.83 mHz) exist in TEC variation at the epicenter region, but do not appear in the far field, which may be caused by the attenuation with the disturbance propagation. The most disturbed direction is the northwest and southeast, which is perpendicular to the rupture approximately. The directional features seem to be dominated by the sea level vertical displacement caused by the earthquake generated tsunami in the near field.

References

Afraimovich, E. L., N. P. Perevalova, A. V. Plotnikov, and A. M. Uralov (2001), The shock-acoustic waves generated by earthquakes, *Ann. Geophys.,* *19*, 395–409.
Afraimovich, E. L., F. Ding, V. V. Kiryushkin, E. I. Astafyeva, S. Jin, and V. A. Sankov (2010), TEC response to the 2008 Wenchuan earthquake in comparison with other strong earthquakes, *Int. J. Remote Sens.,* *31*(13), 3601–3613.

Artru, J., P. Lognonné, and E. Blanc (2001), Normal modes modelling of post-seismic ionospheric oscillations, *Geophys. Res. Lett.*, *28*(4), 697–700, doi:10.1029/2000GL000085.

Artru, J., T. Farges, and P. Lognonné (2004), Acoustic waves generated from seismic surface waves: Propagation properties determined from Doppler sounding observations and normal-mode modelling, *Geophys. J. Int.*, *158*(3), 1067–1077.

Calais, E., and J. B. Minster (1995), GPS detection of ionospheric perturbations following the January 17, 1994, Northridge earthquake, *Geophys. Res. Lett.*, *22*(9), 1045–1048, doi:10.1029/95GL00168.

Ducic, V., J. Artru, and P. Lognonné (2003), Ionospheric remote sensing of the Denali Earthquake Rayleigh surface waves, *Geophys. Res. Lett.*, *30*(18), 1951, doi:10.1029/2003GL017812.

Dautermann, T., E. Calais, J. Haase, and J. Garrison (2007), Investigation of ionospheric electron content variations before earthquakes in southern California, 2003–2004, *J. Geophys. Res.*, *112*, B02106, doi:10.1029/2006JB004447.

Ekström, G., M. Nettles, and A. M. Dziewonski (2012), The global CMT project 2004-2010: Centroid-moment tensors for 13,017 earthquakes, *Phys. Earth Planet. Inter.*, *200-201*, 1–9, doi:10.1016/j.pepi.2012.04.002.

Galvan, D. A., A. Komjathy, M. P. Hickey, P. Stephens, J. Snively, Y. Tony Song, and A. J. Mannucci (2012), Ionospheric signatures of Tohoku-Oki tsunami of March 11, 2011: Model comparisons near the epicenter, *Radio Sci.*, *47*, RS4003, doi:10.1029/2012RS005023.

Heki, K., and J. Ping (2005), Directivity and apparent velocity of the coseismic ionospheric disturbances observed with a dense GPS array, *Earth Planet. Sci. Lett.*, *236*(3), 845–855.

Heki, K., and Y. Enomoto (2013), Preseismic ionospheric electron enhancements revisited, *J. Geophys. Res. Space Phys.*, *118*, 6618–6626, doi:10.1002/jgra.50578.

Heki, K., et al. (2006), Detection of ruptures of Andaman fault segments in the 2004 great Sumatra earthquake with coseismic ionospheric disturbances, *J. Geophys. Res.*, *111*, B09313, doi:10.1029/2005JB004202.

Jin, S. G., P. H. Park, and W. Y. Zhu (2007), Micro-plate tectonics and kinematics in Northeast Asia inferred from a dense set of GPS observations, *Earth Planet. Sci. Lett.*, *257*(3-4), 486–496, doi:10.1016/j.epsl.2007.03.011.

Jin, S., O. F. Luo, and P. Park (2008), GPS observations of the ionospheric F2-layer behavior during the 20th November 2003 geomagnetic storm over South Korea, *J. Geod.*, *82*(12), 883–892.

Jin, S. G., W. Y. Zhu, and E. Afraimovich (2010), Co-seismic ionospheric and deformation signals on the 2008 magnitude 8.0 Wenchuan Earthquake from GPS observations, *Int. J. Remote Sens.*, *31*(13), 3535–3543, doi:10.1080/01431161003727739.

Liu, J. Y., Y. J. Chuo, S. J. Shan, Y. B. Tsai, Y. I. Chen, S. A. Pulinets, and S. B. Yu (2004), Pre-earthquake ionospheric anomalies registered by continuous GPS TEC measurements, *Ann. Geophys.*, *22*(5), 1585–1593.

Liu, J. Y., C. H. Chen, C. H. Lin, H. F. Tsai, C. H. Chen, and M. Kamogawa (2011), Ionospheric disturbances triggered by the 11 March 2011 M9.0 Tohoku earthquake, *J. Geophys. Res.*, *116*, A06319, doi:10.1029/2011JA016761.

Lognonné, P., J. Artru, R. Garcia, F. Crespon, V. Ducic, E. Jeansou, G. Occhipinti, J. Helbert, G. Moreaux, and P.-E. Godet (2006), Ground-based GPS imaging of ionospheric post-seismic signal, *Planet. Space Sci.*, *54*(5), 528–540.

Kakinami, Y., M. Kamogawa, Y. Tanioka, S. Watanabe, A. R. Gusman, J. Y. Liu, Y. Watanabe, and T. Mogi (2012), Tsunamigenic ionospheric hole, *Geophys. Res. Lett.*, *39*, L00G27, doi:10.1029/2011GL050159.

Klobuchar, J. A. (1987), Ionospheric time-delay algorithm for single-frequency GPS users, *IEEE Trans. Aerosp. Electron. Syst.*, *AES-23*(3), 325–331.

Mansoori, A. A., P. A. Khan, P. Bhawre, A. K. Gwal, and P. K. Purohit (2013), Variability of TEC at mid latitude with solar activity during the solar cycle 23 and 24, in *Proceedings of 2013 IEEE International Conference on Space Science and Communication*, pp. 83–87.

Matsumura, M., et al. (2011), Numerical simulations of atmospheric waves excited by the 2011 off the Pacific coast of Tohoku Earthquake, *Earth Planets Space*, *63*(7), 885–889.

Occhipinti, G., L. Rolland, P. Lognonné, and S. Watada (2013), From Sumatra 2004 to Tohoku-Oki 2011: The systematic GPS detection of the ionospheric signature induced by tsunamigenic earthquakes, *J. Geophys. Res. Space Physics*, *118*, 3626–3636, doi:10.1002/jgra.50322.

Rolland, L. M., P. Lognonné, and H. Munekane (2011), Detection and modeling of Rayleigh wave induced patterns in the ionosphere, *J. Geophys. Res.*, *116*, A05320, doi:10.1029/2010JA016060.

Saito, A., T. Tsugawa, Y. Otsuka, M. Nishioka, T. Iyemori, M. Matsumura, and N. Choosakul (2011), Acoustic resonance and plasma depletion detected by GPS total electron content observation after the 2011 off the Pacific coast of Tohoku Earthquake, *Earth Planet. Space*, *63*(7), 863–867.

Shinagawa, H., T. Tsugawa, M. Matsumura, T. Iyemori, A. Saito, T. Maruyama, H. Jin, M. Nishioka, and Y. Otsuka (2013), Two-dimensional simulation of ionospheric variations in the vicinity of the epicenter of the Tohoku-oki earthquake on 11 March 2011, *Geophys. Res. Lett.*, *40*, 5009–5013, doi:10.1002/2013GL057627.

Tsugawa, T., A. Saito, Y. Otsuka, M. Nishioka, T. Maruyama, H. Kato, T. Nagatsuma, and K. T. Murata (2011), Ionospheric disturbances detected by GPS total electron content observation after the 2011 off the Pacific coast of Tohoku Earthquake, *Earth Planets Space*, *63*(7), 875–879.